Clays and Clay Minerals, Vol. 63, No. 5, 337–350, 2015.

CEC AND ^{7}Li MAS NMR STUDY OF INTERLAYER Li^{+} IN THE MONTMORILLONITE–BEIDELLITE SERIES AT ROOM TEMPERATURE AND AFTER HEATING

ANNETT STEUDEL[1], RALF HEINZMANN[2], SYLVIO INDRIS[3], AND KATJA EMMERICH[1,4]

[1] Institute of Functional Interfaces (IFG), Karlsruhe Institute of Technology, Hermann-von-Helmholtz-Platz 1, D-76344 Eggenstein-Leopoldshafen, Germany
[2] Bruker Biospin GmbH, Silberstreifen 4, 76287 Rheinstetten, Germany
[3] Institute of Applied Materials – Energy Storage Systems (IAM-ESS), Karlsruhe Institute of Technology, Hermann-von-Helmholtz-Platz 1, D-76344 Eggenstein-Leopoldshafen, Germany
[4] Competence Center for Material Moisture (CMM), Karlsruhe Institute of Technology, Hermann-von-Helmholtz-Platz 1, D-76344 Eggenstein-Leopoldshafen, Germany

Abstract—The objective of the study was to contribute to the understanding of the influence of the structure and the 2:1 layer dimension of smectites on cation exchange capacity (CEC) reduction and the hydration behavior of Li-saturated smectites after heating. Five montmorillonites extracted from bentonites of different provenance were saturated with Li^{+} and heated to 300ºC. Initial montmorillonites and montmorillonites with reduced layer charge (RCM) were characterized by comprehensive mineralogical analysis supplemented by CEC measurements, surface-area measurements by Ar adsorption, and ^{7}Li, ^{27}Al, and ^{29}Si magic-angle spinning nuclear magnetic resonance spectroscopy (MAS NMR). The CEC of the initial montmorillonites varied between 89 and 130 cmol(+)/kg while the CEC of the RCM prepared at 300ºC varied between 8 and 25 cmol(+)/kg. The lateral dimension of the 2:1 layers varied between 70 and 200 nm. The greatest decrease in CEC was observed for the montmorillonite with the largest diameter of the 2:1 layers and the smallest decrease was observed for the montmorillonite with the smallest diameter of the 2:1 layers. ^{7}Li MAS NMR revealed an axially symmetric chemical environment of the hydrated interlayer Li^{+} with $\eta_{\Delta} = 0$ for the chemical shift anisotropy tensor for unheated montmorillonites with >33% tetrahedral layer charge (ξ). The chemical environment is typical of inner-sphere hydration complexes of interlayer Li^{+}. An axially non-symmetric chemical environment of the interlayer Li^{+} with ηCS of close to one was observed for all RCM. While the remaining CEC of RCM prepared at 300ºC reflected the variable CEC at the edges, and thus the lateral size or aspect ratio of the 2:1 layers, the hydration complex of interlayer Li^{+} was strongly determined by the isomorphic substitutions in the dioctahedral 2:1 layers.

Key Words—^{27}Al MAS NMR, Cation Exchange Capacity, Edge Charge, Hydration, Layer Charge, ^{7}Li MAS NMR, Montmorillonite, ^{29}Si MAS NMR, Smectites.

INTRODUCTION

Smectites and bentonites are often used in natural form for industrial purposes (Eisenhour and Brown, 2009; Harvey and Lagaly, 2013). For specific applications, treatment of smectites such as homoionic exchange possibly followed by heating (Mosser *et al*., 1997; Emmerich *et al*., 1999, 2001; Karakassides *et al*., 1999; Madejová *et al*., 2000; Hrobáriková and Komadel, 2002; Skoubris *et al*., 2013) or modification with acid (Novák and Čičel, 1978; Komadel *et al*., 1997; Steudel *et al*., 2009), alkaline (Carroll and Starkey, 1971; Jozefaciuk and Bowanko, 2002; Becerro *et al*., 2009), or organic solutions (Breen *et al*., 1997; Xi *et al*., 2004; Betega de Paiva *et al*., 2008) is necessary to increase the value of the product. Within this general approach, a comprehensive evaluation of the smectite is essential for performance assessment of both the natural and treated material. Smectites show a large variability in chemical composition, layer charge (ξ), and layer-charge density (Emmerich *et al*., 2009; Wolters *et al*., 2009) due to the substitutions in the octahedral and tetrahedral sheets.

In the first part of the study, special attention was paid to the classification of the initial samples as dioctahedral smectites according to Emmerich *et al*. (2009). The classification considered the *cis*- and *trans*-vacant character of the octahedral sheet, the ξ and, the tetrahedral charge.

Heating at 200–300ºC of Li^{+}-exchanged dioctahedral smectites induces fixation of interlayer Li^{+} (Hofmann-Klemen effect – Hofmann and Klemen 1950), supposedly in a structure similar to hectorite, but accompanied by greatly reduced cation exchange capacity (CEC) and an irreversible loss of hydration capacity. Montmorillonites with reduced CEC are often referred to as montmorillonites with reduced layer charge.

Two main models have emerged to explain the reaction mechanism of the Hofmann-Klemen effect:

* E-mail address of corresponding author:
annett.steudel@kit.edu
DOI: 10.1346/CCMN.2015.0630501

migration of Li^+ into (1) the vacancies of the montmorillonite octahedral sheets or (2) the bottom of the pseudohexagonal cavities in the tetrahedral sheet at the basal surfaces of the montmorillonite.

Fourier transform infrared spectroscopy (FTIR) revealed that most Li^+ ions migrate upon heating into the octahedral vacancies and create local trioctahedral AlMgLiOH groups (Calvet and Prost, 1971; Sposito *et al*., 1983; Madejová *et al*., 1996, 2000; Gates *et al*., 2000; Skuobris *et al*., 2013).

In contrast, ^7Li MAS NMR results indicated that Li^+ did not migrate into the vacant octahedral sites but rather into the bottom of the pseudohexagonal cavities of the tetrahedral sheets (Luca *et al*., 1989; Theng *et al*., 1997) and collapsed Li-saturated montmorillonite re-expands under high water-vapor pressures up to 8.5 MPa (Alvero *et al*., 1994; Alba *et al*., 1998).

In all RCM and Li^+ fixation studies, the CEC after heating to 250−300ºC was reduced to values between 2 and 51 cmol(+)/kg, corresponding to decreases in CEC of between 98.5 and 54% of the initial CEC (Jaynes and Bigham, 1987; Bujdák *et al*., 1991; Theng *et al*., 1997; Madejová *et al*., 1999; Gates *et al*., 2000; Hrobáriková *et al*., 2001; Skoubris *et al*., 2013), respectively. Despite the known structural parameters (high octahedral charge and low Fe content; Komadel *et al*., 2005) that determine the charge reduction qualitatively, the quantitative prediction of CEC reduction in relation to the initial CEC is not yet possible. Previously, the influence of the lateral layer dimension and the influence of the aspect ratio on the CEC at the edges have been ignored. Unfortunately, only a few studies used more than two samples (Jaynes and Bigham, 1987; Hrobáriková *et al*., 2001).

The aim of the present study was to contribute to the understanding of CEC reduction and related changes in hydration behavior observed for heated Li-saturated smectites as they depend on structure and 2:1 layer dimension. For this purpose, in the second part of the study, ^7Li NMR MAS was used to study the interlayer Li^+ of five dioctahedral smectites and the RCM.

MATERIAL

Five technical bentonites (BP, BE, BV, BC, and BI) were investigated. Bentonite BC is comparable to Calcigel (referred to as Montigel in early publications), bentonite BV is similar to Volclay and MX-80, and bentonite BE is comparable to the Spanish bentonite from Gabo de Gata (Almeria). Bentonite BI comes from India and no studies of this material exist. The provenance of bentonite BP is unknown. The material was provided by Clariant Produkte (Deutschland) GmbH (formerly SÜD-CHEMIE AG). The smectites of these bentonites differ in chemical composition, structure, and layer dimension. In this paper, the samples are listed with increasing net layer charge in the tetrahedral sheet. X-ray diffraction (XRD) analysis revealed that the samples contained dioctahedral smectites of the montmorillonite–beidellite series. The smectites varied in terms of ξ, tetrahedral charge, octahedral structure, and Fe(II/III) content according to pre-test screening. Screening included ξ measurements according to Olis *et al*. (1990), X-ray fluorescence (XRF) measurements, and simultaneous thermal analysis (STA) of the bulk material.

All samples were purified as described by Mehra and Jackson (1960), Tributh and Lagaly (1986a, 1986b), and Wolters *et al*. (2009) before separating the <2 µm fraction by sedimentation to enrich the montmorillonite (BP-M2, BE-M2, BV-M2, BC-M2, and BI-M2). Purification included 12 washing steps with 1 M NaCl solution (Merck KGaA, Darmstadt, Germany) to remove excess reactants. The Na^+ concentration in the washing solution equaled 20 to 30 times the CEC of the smectite; the washing ensured homoionic saturation of all montmorillonites and beidellites, therefore (Steudel and Emmerich, 2013). The solid concentration for fractionation by sedimentation was <1%. The purified Na^+-exchanged <2 µm fraction (BP-M2Na, BE-M2Na, BV-M2Na, BC-M2Na, and BI-M2Na) was then exchanged homoionically with Li^+ (using LiCl solution; Merck KGaA, Darmstadt, Germany) following Steudel and Emmerich (2013). The concentration of the LiCl solution was 20 times the CEC of the smectite. The Li^+-exchanged materials (BP-M2Li, BE-M2Li, BV-M2Li, BC-M2Li, and BI-M2Li) were divided into five portions of 5 g each. One subsample of each material was kept at room temperature (R*T*), while the other subsamples were calcinated for 24 h at each of several temperatures (110, 150, 200, and 300ºC) in air to obtain RCM (Bujdák *et al*., 1991; Madejová *et al*., 1996, 2000; Hrobáriková *et al*., 2001; Komadel, 2003). The samples were stored in closed tubes under laboratory conditions (22ºC, 40% r.h.).

METHODS

The smectite content of the <2 µm fractions and the hydration state under ambient conditions were determined by XRD analysis of powdered samples (top loading) using a Siemens D5000 diffractometer (Bruker AXS GmbH Karlsruhe, Germany; CuKα radiation, goniometer radius = 220.5 mm, tube focus = 12 mm × 0.04 mm, voltage = 40 mV, current = 40 mA, graphite secondary monochromator, divergence and antiscatter slit at 1 mm, detector slit = 0.1 mm). Data were recorded between 5 and 80º2θ with a 3 s counting time per 0.02º2θ step, Quantitative analysis was performed using the Rietveld software *Autoquan* (Agfa NDT Pantak Seifert GmbH_Co.KG, Ahrensburg, Germany, Version 2.7.0) (Kleeberg and Bergmann, 2002). The mineral names were abbreviated according to Whitney and Evans (2010).

https://doi.org/10.1346/CCMN.2015.0630501 Published online by Cambridge University Press

For the Greene-Kelly (GK) test (Greene-Kelly, 1952), the RCM samples heated at 300ºC were used. The powders (50 mg) were suspended in deionized water (1.5 mL). The suspensions were treated with the ultrasonic finger (UP 200s, Hielscher Ultrasonics GmbH, Teltow, Germany; amplitude: 90, cycle: 0.9) for 1 min to yield a homogenous suspension. Afterward, the suspensions were pipetted onto glass slides and dried at R*T* under atmospheric conditions. The oriented samples were measured when air-dried and after treatment with glycerol. The oriented samples were stored for 5 days in a desiccator above glycerol (anhydrous, Roth GmbH & Co. KG, Karlsruhe, Germany) at 110ºC in a drying oven. The positions of the basal (001) and the 002/004 diffraction peaks in the air-dried and glycerol-treated pattern were examined (Schultz, 1969). The difference between the 002 peak of the unexpanded montmorillonite (0.48 nm) and the 004 peak of the glycerol-expanded beidellite (0.45 nm) was used to determine the percentage of net ξ in the tetrahedral sheet (Schultz, 1969).

The ξ was determined by the alkyl ammonium method (Lagaly and Weiss, 1971; Lagaly, 1994) using 14 alkyl ammonium solutions (Sigma-Aldrich Chemie GmbH, Steinhein, Germany) of varying alkyl chain length from $n_C = 4$ to $n_C = 18$ (Steudel, 2009; Wolters *et al*., 2009).

Mössbauer spectroscopy was applied to the Na^+-exchanged samples (BP-M2Na, BE-M2Na, BV-M2Na, BC-M2Na, BI-M2Na) to identify the valence state and the ratio of Fe(III) and Fe(II) and to distinguish between silicate-bound Fe(II/III) and oxide-bound Fe(II/III). Mössbauer spectra were recorded at 298 K and 4.2 K with a standard transmission spectrometer (in-house construction with components from Halder Electronics, Germany), using a ^{57}Co source in a rhodium matrix and a sinusoidal velocity waveform. The X-rays were detected with a krypton/CO_2 proportional counter (Wagner and Kyek, 2004; Wolters, 2005; Petrick, 2011). The software *MFit* (Version 1.0 alpha/2 Win 32) was used to evaluate all Mössbauer spectra. The Mössbauer measurements at R*T* (298 K) were fitted with one or two doublets attributed to octahedral Fe(III) and octahedral Fe(II) as well as with one sextet with a magnetic hyperfine field (B_{HF}) of 50.2 T, an isomer shift (IS) of 0.26 mm/s, and a quadrupole splitting (QS) of −0.21 mm/s, indicating the presence of hematite (Murad and Schwertmann, 1986; Murad and Johnston, 1987). The magnetic hyperfine field decreased with increasing Al substitution (up to 10%) and with decreasing crystal size (Murad and Schwertmann, 1986; Murad and Johnston, 1987). An additional sextet that is attributed to paramagnetic relaxation was implemented to fit the baseline (Fysh *et al*., 1983; Murad, 1998).

The chemical composition of the Na^+-saturated montmorillonites was determined by XRF. The analyses were performed using a Phillips MagiXPRO spectrometer (PANalytical B.V., Almelo, Netherlands; company of Spectris plc., Egham, England) equipped with a rhodium X-ray tube (stimulation power: 3.2 kW) using air-dried powdered samples fused with lithium tetraborate (mixing ratio 1:7; Merck KGaA, Darmstadt, Germany). The loss on ignition was determined separately at 1000ºC (2 h). The stoichiometric elemental composition of the smectites was calculated from the XRF analyses according to Köster (1977). The calculation is based on the assumption of 22 negative charges [$O_{10}(OH)_2$] and involved the measured ξ (Wolters *et al*., 2009). In spite of purification and separation, some smectite samples contained small amounts of accessory phases, which were quantified by XRD. The XRF analyses were corrected accordingly,

The CEC was measured with 0.01 M Cu-triethylenetetramine (Cu-trien; using 0.1 M $CuSO_4$ solution from Merck KGaA, Darmstadt, Germany and triethylenetetramine from Sigma-Aldrich Chemie GmbH, Steinhein, Germany; Meier and Kahr, 1999; Steudel *et al*., 2009; Wolters *et al*., 2009). All CEC values were normalized to the montmorillonite content. The exchanged cations in the supernatant were subsequently analyzed by inductively-coupled plasma optical-emission spectroscopy (ICP-OES, Type OPTIMA 8300 DV; PerkinElmer Inc., Waltham, Massachusetts, USA) to assess the saturation of the interlayer by Li^+ (Steudel and Emmerich, 2013).

The hydration state and the *cis*- and *trans*-vacant character of the dioctahedral smectites was estimated by applying STA (Wolters and Emmerich, 2007; Wolters *et al*., 2009; Emmerich, 2011). The water content (w_{min}) was determined using the thermogravimetric (TG) curve in the range between R*T* and 300ºC. The *cis*- and *trans*-vacant character (Drits *et al*., 1995; Wolters and Emmerich, 2007; Wolters *et al*., 2009) of the octahedral sheet was determined by peak deconvolution of the mass spectrometer curve of evolved water (m/z = 18) in the range between 350 and 900ºC using *PeakFit* (Version 4.12; SeaSolve Software, Framingham, Massachusetts, USA). The smectites were classified according to Emmerich *et al*. (2009).

The specific surface area (A_S) was measured by Ar adsorption using a Quantachrome Autosorb-1MP (Quantachrome GmbH & Co. KG, Odelzhausen, Germany) and the Brunauer-Emmet-Teller (BET) method (Brunauer *et al*., 1932; Gregg and Sing, 1991). Between six and eight adsorption points in the linear range of p/p_0 from 0.03 and 0.32 were used for BET evaluation. The outgassing conditions were 24 h under vacuum at 95ºC. The pressure, which was reached after outgassing, was ~1 mbar.

A_S was the sum of the basal specific surface area ($A_{S,basal}$) and the edge specific surface area ($A_{S,edge}$). The $A_{S,basal}$ is dependent on the number of layers per stack (n) and the $A_{S,edge}$ depends on the square length (L) of the particles. The number of layers per stack (n)

https://doi.org/10.1346/CCMN.2015.0630501 Published online by Cambridge University Press

decreases with increasing A_S and constant L. The square length (L) of the particles decreases with increasing A_S and constant n. The A_S was used to determine the range of L and n for each sample. The square length (L) was used to calculate the perimeter (U) and the basal area ($A_{S,basal}$) of the clay particles. Together with the density (ρ_s of 2.7 g/cm^3) of the smectite particles, the edge surface area ($A_{S,edges}$) was calculated according to the following formula:

$$A_{S,edges} = \frac{U}{\rho \cdot A_{S,basal}} [m^2/g] \quad (1)$$

The thickness of one layer of dehydrated smectite was fixed at 0.95 nm. The structural formula reflects the substitutions in the tetrahedral and octahedral sheets. The amounts of Al substituted for Si in the tetrahedral sheet (y) and of Mg or Fe(II) for Al in the octahedral sheet (x) were applied to calculate the site densities of the tetrahedral (N_T) and octahedral (N_O) sheet according to White and Zelazny (1988), Tournassat *et al*. (2003), and Delavernhe *et al*. (2015).

The sum of both equates to the total amount of formal sites (White and Zelazny, 1988; Tournassat *et al*., 2003; Delavernhe *et al*.; 2015), which were compared with the CEC measurements of the Li-saturated material after heating at 300ºC.

^{7}Li, ^{27}Al, and ^{29}Si MAS NMR spectroscopy was performed at R*T* on a Bruker Avance spectrometer (Bruker BioSpin GmbH, Rheinstetten, Germany) with a field of 7.05 T. The ^{7}Li, ^{27}Al, and ^{29}Si MAS NMR spectra were obtained at 116.7 MHz, 78.3 MHz, and 59.7 MHz, respectively. The MAS NMR measurements were done with 4 mm rotors at a spinning speed of 10 kHz in dry nitrogen atmosphere. Chemical shifts (δ) for ^{7}Li, ^{27}Al, and ^{29}Si were referenced to 1 M LiCl solution (Merck KGaA, Darmstadt, Germany), 1 M $Al(NO_3)_3$ solution (Merck KGaA, Darmstadt, Germany), and pure tetramethylsilane (TMS; Merck KGaA, Darmstadt, Germany), respectively. The typical value for the recycling delay of ^{7}Li, ^{27}Al, and ^{29}Si was 5 s. ^{7}Li and ^{29}Si MAS NMR experiments were performed with a rotor-synchronized Hahn-echo sequence ($\pi/2-\tau-\pi-\tau-$acquisition) and a typical $\pi/2$ pulse length of 2 µs. ^{27}Al MAS NMR experiments were recorded with a one-pulse experiment ($\pi/18-$acquisition). Due to the large quadrupole moment of Al, a $\pi/18$ pulse length of <0.9 µs was used. The software *DMFit* (2011, developed by Dominique Massiot, Orléans, France, http://nmr.cemhti.cnrs-orleans.fr/Dmfit/Howto/CSA/CSA_MAS.aspx) was used to evaluate all MAS NMR spectra (Massiot *et al*., 2002). ^{29}Si MAS NMR spectra were fitted with Gaussian lines. The spinning sidebands (ssb) were evaluated with the ssb model of the *DMFit* program. The maxima of the ^{27}Al MAS NMR resonances were also determined by using Gaussian lines. ^{7}Li MAS NMR spectra were fitted with one peak for the main resonance signal using a Gaussian/Lorentzian line and one peak for each ssb using the ssb model of the *DMFit* program. In addition, the ^{7}Li MAS NMR spectra were fitted with the chemical shift anisotropy magnetic resonance spectroscopy (CSA MAS) model of *DMFit*. As well as spinning rate, the simulation results involved isotropic position, the width of the resonance signal, and information about the CSA tensor. The chemical shift tensor describes the electric field surrounding the atom with the principle components of the tensor; δ_{xx}, δ_{yy}, δ_{zz} (standard convention: δ_{11}, δ_{22}, δ_{33}) and can be represented by a 3-by-3 matrix. The parameter ΔCS [ppm] reveals the axiality of the CSA tensor (Bak *et al*., 2000; Massiot *et al*., 2002). The values of ΔCS can vary in all three directions. If two values are equal, the system is axially symmetric. The parameter ηCS gives information about the symmetry of the environment around the atom and is in the range between 0 (symmetric) and 1 (asymmetric) (Bak *et al*., 2000; Massiot *et al*., 2002).

RESULTS AND DISCUSSIONS

Mineralogy of separated clay fraction and structural formula of pure smectites

The XRD powder pattern (Figure 1) of the Li^+-saturated <2 µm fraction showed a first basal diffraction peak (d_{001}) between 1.24 and 1.33 nm and a d_{060} value between 0.1495 and 0.1500 nm, indicating dioctahedral smectites (Sme_{di}). All samples excluding BI-M2Li contain SiO_2 impurities indicated by peaks at 0.405 nm and 0.334 nm, typical of cristobalite (Crs) and quartz (Qz), respectively. The powder patterns of BI-M2Li and BC-M2Li (Figure 1) showed peaks at 0.715 nm and 1.01 nm which revealed the presence of kaolinite (Kln) and mica (Ms) that were pronounced in the pattern of oriented samples. The mica content correlated well with the amount of potassium determined by XRF. No crystalline Fe oxide and Fe hydroxide phases were identified by XRD.

Rietveld quantification yielded smectite contents of between 71 and 99% for the Li^+-saturated materials (Table 1). The quantification results of the Na^+-exchanged smectites (data not shown) were similar to those of the Li^+-exchanged smectites. No loss of fine-grained smectite occurred during Li^+ exchange.

Mössbauer measurements revealed oxide-bound Fe(II/III) contents of ~5% of total Fe content for BE-M2 and BI-M2. Only three of five samples (BP-M2, BV-M2, and MC-M2) contained silicate-bound Fe(II) between 4.5 and 11.7% of total Fe content. The resulting abundances of FeO were <0.5%. The structural formula for each dioctahedral smectite could be calculated based on the results of the Rietveld analysis, Mössbauer spectroscopy, and ξ measurements (Table 2). Small deviations from previously published formulae for the samples (Steudel *et al*., 2009; Wolters *et al*., 2009) can be explained by the use of different batches of starting

https://doi.org/10.1346/CCMN.2015.0630501 Published online by Cambridge University Press

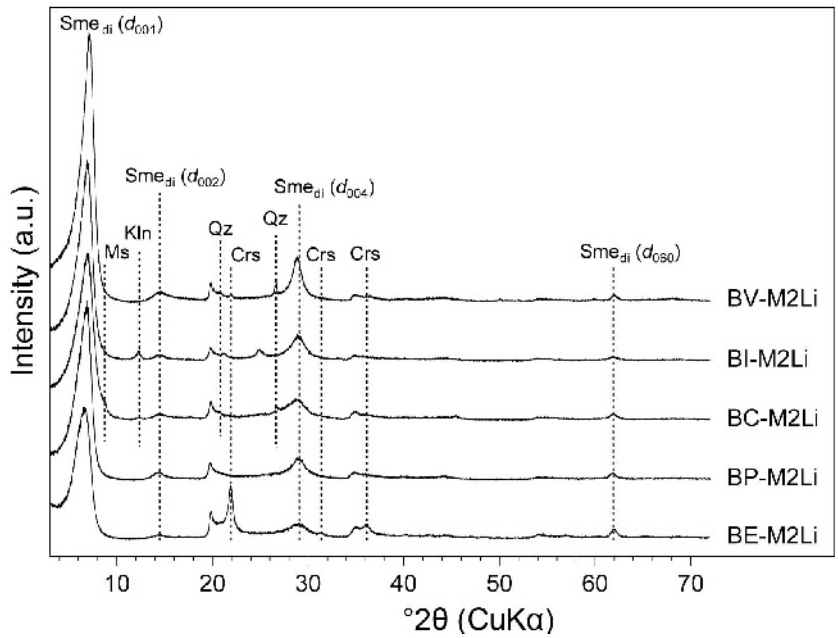

Figure 1. XRD pattern of powdered samples of the Li-saturated <2 μm fraction (Sme_{di} – dioctahedral smectite; Crs – cristobalite; Kln – kaolinite; Ms – muscovite; Qz – quartz).

materials and different particle-size fractions (<2 μm and <0.2 μm) studied.

Tetrahedral charges derived from structural formulae increased from 12% (BP-M2Na) to 35% (BC-M2Na) and correspond well with the results from the GK test (Table 2). For sample BP-M2Na the tetrahedral charge is just at the transition from montmorillonite to beidellitic montmorillonite. Sample BI-M2Na was classified as montmorillonitic beidellite although the deviation between tetrahedral charge from structural formula (79%) and GK test (55%) was larger (Table 2). Only one sample, BVM2-Li, was completely *cis*-vacant. The other four smectite samples possessed different amounts of *trans*-vacant octahedral positions. The sample BC-M2Li had nearly equal *cis*- and *trans*-vacant shares. Both samples BE-M2Li and BP-M2Li contained the same amounts of *cis*- and *trans*-vacant octahedral positions and belong to the group of *cis*-*trans*-vacant smectites (Wolters and Emmerich, 2007). The sample BI-M2Li had more *trans*-vacant positions and can be assigned to the group of *trans*-*cis*-vacant smectites (Table 2).

Exchange and surface properties of the Li^+-exchanged smectites

The CEC of the smectites varied between 89 and 132 cmol(+)/kg. The analysis of the interlayer occupancy revealed Li concentrations of between 89 and 96%, which proved that the homoionic exchange procedure was successful (Table 3). The residual interlayer cations are Na > K > Mg > Ca. Basal peaks of the powder diffraction pattern revealed mainly one-layer hydrates. Sample BE-M2Li (d_{001} = 1.33 nm) showed few two-layer hydrates in the interlayer (Figure 1). The A_S varied between 58 and 120 m^2/g (Table 3). The lateral layer dimension (expressed as square length; *L*) varied between 70 and 200 nm (Table 3).

With increasing temperature, the CEC decreased (Table 4) for all Li^+-saturated dioctahedral smectites. BP-M2Li had already lost 77% of CEC at 150ºC and 90% of CEC at 300ºC. BI-M2Li lost only 46% of the CEC at 150ºC and 74% of the CEC at 300ºC. The decrease in the CEC values of BV-M2Li, BC-M2Li, and BE-M2Li was ~64 ± 1% at 150ºC. The decrease in CEC then varied over the range 81 < CEC < 90% of the initial CEC (Table 4) after heating to 300ºC.

Table 1. Smectite content and impurities of the samples.

Phases	BP-M2Li (wt.%)	BE-M2Li (wt.%)	BV-M2Li (wt.%)	BC-M2Li (wt.%)	BI-M2Li (wt.%)
Smectite	98	72	96	86	94
Quartz/Cristobalite	1	25	3	3	–
Kaolinite	–	1	–	2	5
Mica	1	2	1	9	1

https://doi.org/10.1346/CCMN.2015.0630501 Published online by Cambridge University Press

Table 2. Structural formula per formula unit (FU*) of the Na^+-saturated <2 μm fraction according to Köster (1977) using layer-charge (ξ) measurements and classification of the smectite samples according to Emmerich *et al*. (2009).

	Tetrahedral		Octahedral				ξ	*cv/tv***	Net layer charge in the tetrahedral layer***	Classification and descriptive names
Samples	Si (eq/FU)	Al (eq/FU)	Al (eq/FU)	Fe(III) (eq/FU)	Fe(II) (eq/FU)	Mg (eq/FU)	(eq/FU)	(%)	(%)	
BP-M2Na	3.964	0.036	1.379	0.157	0.021	0.522	0.342	67/33	10	low-charged *cv/tv* montmorillonite
BE-M2Na	3.933	0.067	1.545	0.099	–	0.398	0.339	70/30	20	low-charged *cv/tv* beidellitic montmorillonite
BV-M2Na	3.926	0.074	1.595	0.189	0.009	0.221	0.262	100/0	26	low-charged *cv* beidellitic montmorillonite
BC-M2Na	3.891	0.109	1.334	0.337	0.020	0.373	0.310	56/44	33	low-charged *cv/tv* ferrian beidellitic montmorillonite
BI-M2Na	3.732	0.268	1.266	0.536	–	0.261	0.340	30/70	55	low-charged *cv/tv* ferrian montmorillonitic beidellite

* FU correlates to $[O_{10}(OH)_2]$, *i.e*. half unit cell
** Proportion of *trans*-vacant (*tv*) and *cis*-vacant (*cv*) layers
*** Greene Kelly test (Greene-Kelly, 1955; Schultz, 1969)

All CEC measurements were repeated after 2 y to check whether the incorporation of Li^+ was reversible. The differences in the CEC values were in the range of the error of the methods (± 3 cmol(+)/kg). The incorporation of Li^+ was irreversible and the RCM were stable after storage at ambient conditions (R*T*, 53% r.h.) for >2 y.

The degree of reduction in CEC of the samples studied was compared to the series of RCM of Madejová *et al*. (1999), Hrobáriková *et al*. (2001), and Skoubris *et al*. (2013) (Table 4). The CEC values of the starting materials covered the same range as samples in the present study. The literature data were included to improve the statistical significance. Two large groups of smectites were detected with respect to the decrease in the CEC. For the first group of samples, CEC decreased by between 38 and 49% at 150ºC and by 54−74% at 300ºC while the CEC of the second group decreased more significantly, by between 58 and 77% at 150ºC (with the exception of sample Bent JP) and by between 81 and 90% at 300ºC (Table 4). Comparison of all samples showed that the initial CEC of the unheated Li^+-exchanged material gave no information about the final CEC decrease. Bent SA and BV-M2Li with the same CEC showed huge differences in the decrease of the CEC (Figure S1; Figures S1−S7 have been deposited with the Editor in Chief and are available from www.clays.org/journal/JournalDeposits.html).

Seven samples displayed a linear correlation $y = -132.16\xi + 121.98$ between ξ of the starting smectite and the decrease in CEC but four samples did not fit the correlation at all (data not shown). No straightforward correlation between the CEC of the RCM and either the

Table 3. Interlayer composition, exchange, and surface properties.

Samples	Li^+ (%)	Na^+ (%)	K^+ (%)	Ca^{2+} (%)	Mg^{2+} (%)	A_S (m^2/g)	*L* (nm)	*n*	$CEC_{meas.}$ (cmol(+)/kg)	CEC# (cmol(+)/kg)	$CEC^{\#}_{300ºC}$ (cmol(+)/kg)	Number of formal sites* (cmol(+)/kg)
BP-M2Li	95.5	1.9	0.5	0.5	1.5	110	140	7	122	124	12	12
BE-M2Li	95.9	1.8	0.6	0.5	1.2	94	100	9	95	132	17	17
BV-M2Li	96.1	2.2	0.5	0.5	0.7	58	200	15	85	89	9	9
BC-M2Li	89.4	4.9	2.5	1.3	1.9	120	100	8	87	101	19	17
BI-M2Li	95.3	2.3	0.5	0.5	1.3	103	70	9	99	105	27	24

CEC normalized to the smectite content
* calculated according to Tournassat *et al*. (2003).

https://doi.org/10.1346/CCMN.2015.0630501 Published online by Cambridge University Press

Table 4. CEC and decrease in dependence on the temperature of the <2 μm fraction of different Li^+-exchanged bentonites from several locations.

Temp. (ºC)	BP-M2Li* (cmol(+)/kg)	(%)	BE-M2Li* (cmol(+)/kg)	(%)	BV-M2Li* (cmol(+)/kg)	(%)	BC-M2Li* (cmol(+)/kg)	(%)	BI-M2Li* (cmol(+)/kg)	(%)	Bent KP[1] (cmol(+)/kg)	(%)	Bent Iv[1] (cmol(+)/kg)	(%)	Bent OT[1] (cmol(+)/kg)	(%)	Bent SA[1] (cmol(+)/kg)	(%)	Bent JP[2] (cmol(+)/kg)	(%)	Bent SAz-1[3] (cmol(+)/kg)	(%)
25	124	0	132	0	89	0	101	0	105	0	121	0	110	0	99	0	92	0	71	0	132	0
110	109	12	111	23	71	20	82	19	96	9	–	–	–	–	–	–	–	–	–	–	–	–
150	29	77	46	65	33	63	36	64	57	46	62	49	75	38	42	58	57	38	35	49	55#	41
200	14	89	23	83	12	86	22	78	34	68	46	62	57	48	26	74	43	53	10	89	35	74
300	12	90	17	87	9	90	19	81	27	74	35	71	51	54	19	81	35	62	8	89	40	70

* CEC values normalized to the smectite content
\# average value of the two measurements at 140ºC and 160ºC
[1] Hrobáriková *et al*. (2001)
[2] Madejová *et al*. (1999)
[3] Skoubris *et al*. (2013)

octahedral charge Mg content, Fe(III) content, or tetrahedral charge (Figures S2, S3) could be established as had been postulated by Madejová *et al*. (1999) and Hrobáriková *et al*. (2001) from a smaller set of samples. This leads to the conclusion that no single structural parameter determines the decrease in CEC. The fate of exchangeable cations at the edges is ignored also.

The total number of formal sites (White and Zelazny, 1988; Tournassat *et al*., 2003) and the measured CEC of Li-saturated samples after heating at 300ºC were similar (Table 3). The greatest decrease in CEC was observed for the smectite (BV-M2) with the largest diameter of the 2:1 layers (~200 nm), while the smallest decrease was observed for the smectite (BI-M2) with the smallest diameter of the 2:1 layers (~70 nm). The $CEC_{300ºC}$ reflects the edge charge content because the total number of formal sites is related to the lateral dimension of the layers, *i.e*. the aspect ratio of layers. The interlayers are completely collapsed after heating at 300ºC and cannot be penetrated by water, and thus, interlayer cations cannot be exchanged by Cu-trien during CEC measurements. Only small amounts of Li^+ are exchangeable, and then only at the edges. Differences between the formal sites and the $CEC_{300ºC}$ are in the range of the error of the estimation of lateral layer dimension. If the total number of formal sites is larger than for the $CEC_{300ºC}$, the lateral layer dimension should be larger, and *vice versa*, if the number of formal sites is smaller than the $CEC_{300ºC}$ the lateral layer dimension should be smaller.

Structural differences of the smectites derived from MAS NMR of heated Li^+-exchanged smectites

The ^{29}Si MAS NMR spectra (Figure S4) of the unheated and heated smectite samples showed one main resonance signal in the narrow range between −93 and −89 ppm typical of phyllosilicates which show δ ^{29}Si between −100 and −70 ppm (Mägi *et al*., 1984; Sanz and Serratosa, 1984; Weiss *et al*., 1987; Sanz and Robert, 1992). The ^{29}Si MAS NMR spectra at R*T* and 300ºC (Figure 2) revealed that the δ ^{29}Si of the Fe-poor smectite (BE-M2Li) was lower (more negative) than the δ ^{29}Si of the Fe-rich smectite (BI-M2LI), because with increasing substitutions in the octahedral and tetrahedral sheets the $\delta^{29}Si$ increased to larger values. The ^{29}Si MAS NMR spectra of BE-M2Li (Figure 2) and BV-M2Li (Figure S4) showed an additional minor resonance at −109 ppm and −106 ppm, respectively, indicating tetrahedral Si in Q^4 units attributed to quartz/cristobalite admixtures (Lippmaa *et al*., 1980) that were confirmed by XRD (Table 1). Small amounts of quartz/cristobalite were also found by XRD for BC-M2Li and BP-M2Li (Table 1). In these samples the content was not sufficiently large to detect a distinct resonance signal in the ^{29}Si MAS NMR spectrum. Only the asymmetry of the main resonance signal with a shoulder to lower values indicated an additional Si environment in the spectrum (Breen *et al*., 1995; Alba

https://doi.org/10.1346/CCMN.2015.0630501 Published online by Cambridge University Press

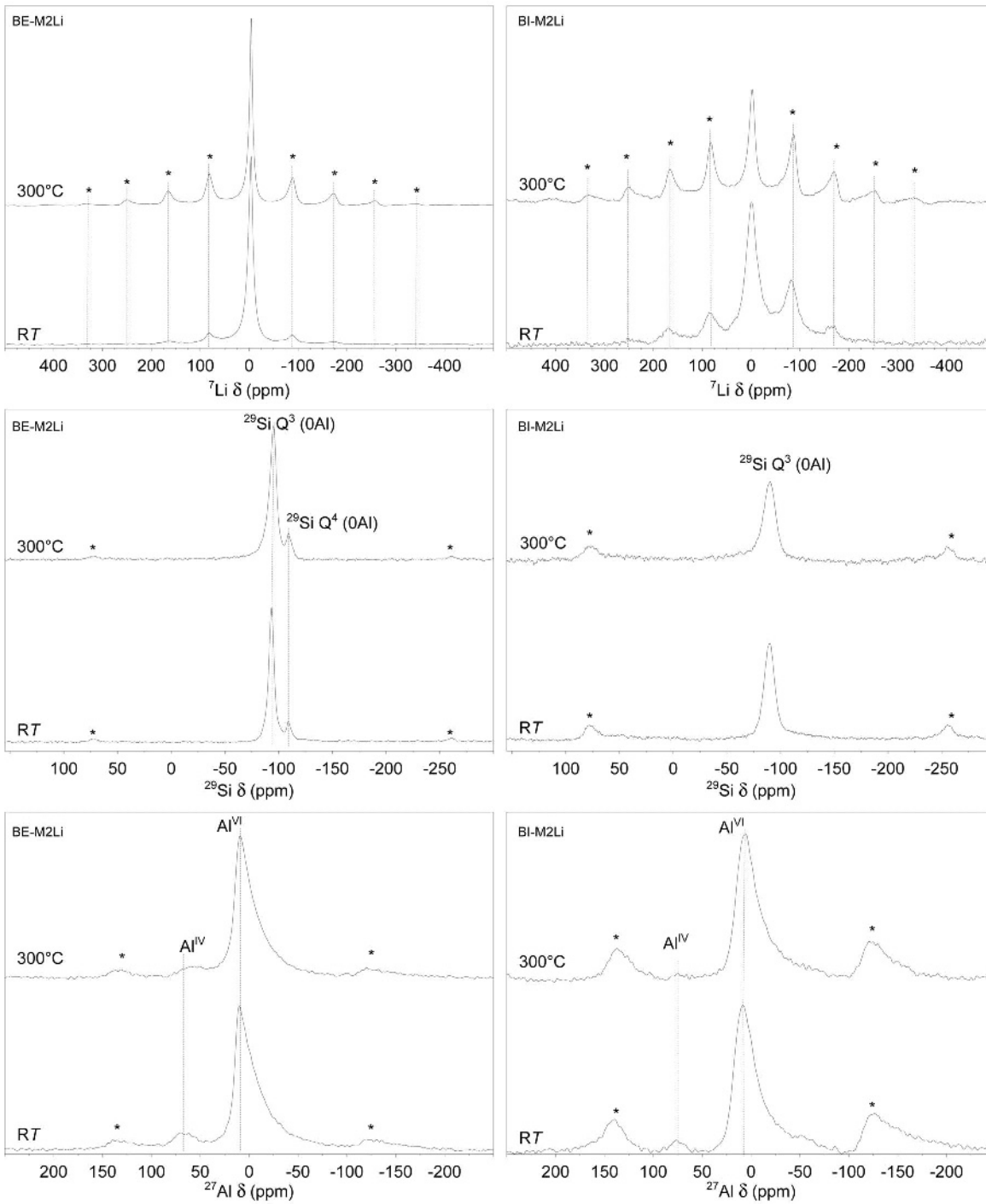

Figure 2. ^{7}Li, ^{29}Si, and ^{27}Al MAS NMR spectra of BE-M2Li (Fe-poor) and BI-M2Li (Fe-rich) at R*T* and 300ºC; * – spinning side bands.

et al., 1998; Cadars *et al*., 2012). No signal for ^{29}Si Q^{3}(1Al) was observed in the ^{29}Si MAS NMR spectra (Figure S4) due to the Fe(II/III)-induced peak broadening and overlapping of the δ^{29}Si (Sanz and Serratosa, 1984). The probabilities of Q^{3} environments depend on the structural formula of the samples (Table 5).

The ^{27}Al MAS NMR spectra (Figure S5) of the unheated samples showed two resonance signals in the ranges between 67.8 and 76.2 ppm and between 6.2 and 10.4 ppm, which revealed tetrahedral (Al^{IV}) and octahedral (Al^{VI}) Al, respectively (Komarneni *et al*., 1986; Tkáč *et al*., 1994; Gates *et al*., 2000). The

https://doi.org/10.1346/CCMN.2015.0630501 Published online by Cambridge University Press

Table 5. Probabilities of Q^3 environments in the tetrahedral sheet based on the structural formula.

Sample	^{29}Si $Q^3(0Al)$ (%)	^{29}Si $Q^3(1Al)$ (%)	^{29}Si $Q^3(2Al)$ (%)	^{29}Si $Q^3(3Al)$ (%)
BP-M2Na	93	7	0	0
BE-M2Na	95	5	0	0
BV-M2Na	95	5	0	0
BC-M2Na	92	8	0	0
BI-M2Na	81	18	1	0

intensity of the Al^{IV} signal is significantly lower and much broader than that of the Al^{VI} signal (Figures 2 and S5) because the amount of Al^{VI} is much greater than that of Al^{IV} (Table 2), confirmed by the structural formula.

The main resonance peak in the spectra of both ^{29}Si and ^{27}Al shifted in the following order of the samples: BE-M2Li < BP-M2Li < BI-M2Li to higher values for the three samples with the same ξ (0.34 eq/FU). This is due to increasing Fe(III) content and substitutions in the octahedral sheet (Mg+Fe(III)) (Sanz and Serratosa, 1984; Weiss *et al*., 1987), which increase in the same order.

All ^7Li MAS NMR spectra of unheated samples (Figure S6) showed one main resonance signal and several ssb. The single resonance indicates only one distinct environment of Li^+ (Alvero *et al*., 1994). The main resonance signal of the five unheated samples was located in the range between −2.9 and −0.9 ppm, which was lower than the δ ^7Li reported by Luca *et al*. (1989), Alvero *et al*. (1994), Theng *et al*. (1997), and Alba *et al*. (1998). The δ ^7Li of the Fe-poor smectite (BE-M2Li) is smaller than the δ ^7Li of the Fe-rich smectite (BI-M2Li) at R*T* and 300ºC (Figure 2). No straightforward correlation between δ^7Li and either the total amount of Li^+ (CEC), octahedral Mg or Fe(III) content could be established. Only the FWHM of the main resonance peak increased exponentially with increasing Fe(III) content.

All NMR spectra (^{29}Si, ^{27}Al, and ^7Li) showed ssb. Sample BE-M2Li (Figure 2) had the smallest Fe(III) content (1.5%) and the ssb were very small but with the greatest signal-to-noise ratio (Oldfield *et al*., 1983; Begaudeau *et al*., 2012). The ssb became more intense with increasing amounts of paramagnetic elements such as Fe(II/III) and as the signal-to-noise ratio decreased (Figure 2).

With increasing temperature, the main resonance signal of ^{29}Si moved to lower values, the main resonance signal of Al^{VI} did not shift and the main resonance signal of Al^{IV} decreased slightly and a small shift of <10 ppm was observed. Similar results were published by Luca *et al*. (1989), Trillo *et al*. (1993), and Gates *et al*. (2000). The shift of the ^{29}Si resonance with increasing temperature is caused by Li^+ fixation resulting in an environment similar to ^{29}Si $Q^4(1Li)$ indicating fixation of Li^+ at the bottom of the pseudohexagonal cavities of the basal surfaces. The decreasing shift of Al^{IV} indicated the fixation of Li^+ at the bottom of the pseudohexagonal cavities of the basal surfaces. Movement of Li^+ into the vacant octahedral sites of the montmorillonite lattice should cause changes in the δ of Al^{VI} but no such changes were observed.

With increased preheating temperature, the main ^7Li resonance moved only slightly between 0.3 and 1.5 ppm (Figure S7). Between 150 and 200ºC the main resonance reached negative values between −1.6 and −3.8 ppm indicating more shielding, *i.e.* a more symmetric environment of Li^+ in the pseudohexagonal cavities, where it is surrounded mainly by Si. At 300ºC a small shift to higher values was observed. This indicates less shielding. The influence of the octahedral sheet, especially the influence of the substitutions (Fe, Mg), increased and caused a more asymmetric environment of Li^+ after heating at 300ºC, because Li^+ entered deeper into the pseudohexagonal cavities.

With increasing temperature, the full width at half maximum (FWHM) of the ^7Li resonance decreased (Table 6) slightly in accordance with the literature (Luca *et al*., 1989; Alvero *et al*., 1994). The observed FWHM values for the unheated and heated samples are one order of magnitude greater than the FWHM of the ^7Li resonance observed for synthetic hectorite (Laponite®) or natural hectorite, both of which contain Li in the octahedral sheet (Luca *et al*., 1989; Theng *et al*., 1997).

If Li^+ migrated into the vacant octahedral sites of the montmorillonite structure, the FWHM of heated montmorillonite should be similar to that of the Laponite or hectorite. The different values suggested that the sites were dissimilar and indicated the migration of Li^+ into

Table 6. FWHM of ^7Li of the Li^+-saturated samples depending on the temperature.

Temp. (ºC)	BP-M2Li (ppm)	BE-M2Li (ppm)	BV-M2Li (ppm)	BC-M2Li (ppm)	BI-M2Li (ppm)
25	19.1	10.4	19.1	25.5	28.9
110	17.9	10.4	16.2	19.7	28.4
150	13.3	9.3	16.2	17.4	16.2
200	11.6	7.5	13.9	15.6	19.7
300	13.3	6.8	13.9	15.6	17.4

https://doi.org/10.1346/CCMN.2015.0630501 Published online by Cambridge University Press

Table 7. Simulation parameter ΔCS used to describe the CSA tensor (Massiot *et al*., 2002); error in ΔCS = ±5 ppm

Sample Temperature (ºC)	BP-M2Li ΔCS (ppm)	BE-M2Li ΔCS (ppm)	BV-M2Li ΔCS (ppm)	BC-M2Li ΔCS (ppm)	BI-M2Li ΔCS (ppm)
25	95	70	95	136	166
110	106	87	103	155	183
150	130	100	126	163	189
200	134	105	129	164	190
300	137	107	134	165	187

the pseudohexagonal cavities of the tetrahedral sheet and not into the octahedral vacancies.

In ^{7}Li MAS NMR spectra with increasing temperature the number of spinning side bands increased (Figure 2), which was caused by lower quadrupole interactions of the dehydrated Li^{+} (Luca *et al*., 1989; Alba *et al*., 1998). Dehydration caused a weaker protection of the Li^{+} and the influence of the atoms in the 2:1 layers increased, which caused the enhancement of the ssb.

To obtain more information about the geometrical environment of the interlayer Li^{+} in a hydrated state and after heating, a CSA analysis was performed and the anisotropy parameter, ΔCS [ppm] (Table 7), and the asymmetry parameter, ηCS [ppm] (Figure 3), which describe the CSA tensor, were considered. The error in ΔCS [ppm] averaged ±5 ppm. The error in ηCS [ppm] was between 0.01 and 0.13 (Figure 3a–e).

The ΔCS values of the unheated samples increased in the following order: BE-M2Li > BV-M2Li = BP-M2Li > BC-M2Li > BI-M2Li due to increasing Fe(III) contents. According to Wolters *et al*. (2009), the Fe(III) content is the dominant factor controlling the octahedral sheet structure of dioctahedral smectites. In addition, the Fe(III) content also influences the amount of tetrahedral substitutions. Both the tetrahedral Al content and the proportion of octahedral *trans* vacancies increased with the amount of Fe(III). ΔCS increased significantly for all samples (by 23–35 ppm) up to a preheating temperature of 150ºC. At higher preheating temperatures, only slight changes of 1 to 5 ppm between the heating steps were observed (Table 7). For samples BC-M2Li and BI-M2Li, ΔCS had increased only slightly (between 6 and 8 ppm) after heating at 110ºC, indicating that dehydration was attained at lower temperatures.

Two samples, BC-M2Li and BI-M2Li, showed ηCS values close to zero indicating a symmetrical chemical environment around Li^{+} in all three spatial dimensions (Figure 3). The detailed assessment of the parameters δ_{11}, δ_{22}, and δ_{33} revealed that BC-M2Li and BI-M2Li showed an axial symmetry around Li, which means that the chemical environment around Li^{+} is equal in two directions. The other three samples (BP-M2Li, BE-M2Li, and BV-M2Li) had ηCS values of between 0.65 and 0.75, which revealed an asymmetrical chemical environment. The chemical environment in all three directions varied, which was also proven by the parameters δ_{11}, δ_{22}, and δ_{33}. For the samples BC-M2Li and BI-M2Li with >33% tetrahedral charge and >44% *trans*-vacant octahedral sheets, the parameter ηCS

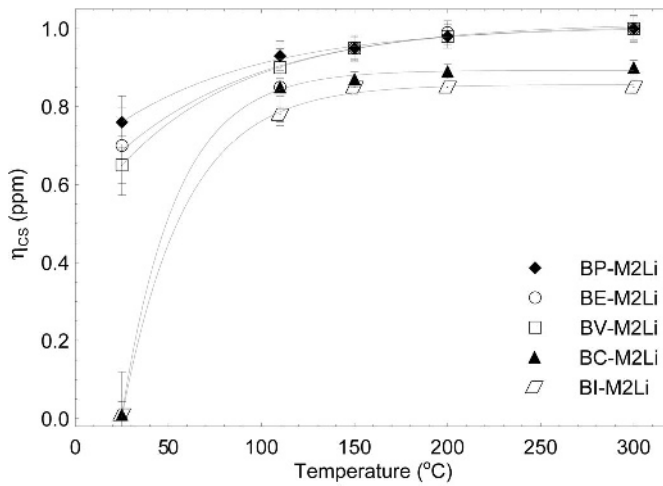

Figure 3. Trend of ηCS *vs*. temperature; ηCS error: 0.01–0.13.

https://doi.org/10.1346/CCMN.2015.0630501 Published online by Cambridge University Press

increased after the first heating step (110ºC) and reached values similar to the samples with lower tetrahedral charge and with a larger amount of *cis*-vacant octahedral sheets (Figure 3).

At R*T*, the Li^+ hydration complexes were kinetically controlled and persistent (ηCS <1). For samples BC-M2Li and BI-M2Li, ηCS was even zero. At higher temperatures, the Li^+ hydration species changed to the thermodynamically stable (fully dehydrated interlayer Li^+) state (ηCS constant between 0.85 and 1). Samples BC-M2Li and BI-M2Li reached the state of thermodynamic stability at lower *T* than the other three samples BP-M2Li, BE-M2Li, and BV-M2Li.

Inner-sphere and outer-sphere hydration complexes of interlayer Li^+ were ascertained concordantly for monolayer hydrated smectites with tetrahedral and octahedral substitutions by Monte Carlo and by molecular dynamics simulations (e.g. Chang *et al*., 1997; Greathouse and Sposito, 1998; Wang *et al*., 2006; Mignon *et al*., 2010). In montmorillonites without tetrahedral substitutions only outer-sphere species were predicted, and inner-sphere species of hydrated Li^+ were determined for beidellites without octahedral substitutions. With increasing ξ, hydrated interlayer Na^+ and Li^+ tend to form inner-sphere complexes for montmorillonite also (Skipper *et al*., 1995; Mignon *et al*., 2010).

The ηCS indicate inner-sphere complexes of hydrated Li^+ with an axial symmetry for the montmorillonite BC-M2Li with 33% of tetrahedral charge. Based on these results, the limits for classification of beidellitic montmorillonites as suggested by Emmerich *et al*. (2009) might have to be shifted from 10% tetrahedral charge to a value between 26 and 33% tetrahedral charge. For all three montmorillonite samples (BV-M2Li, BE-M2Li, and BP-M2Li) with <26% tetrahedral charge, ηCS was much larger than zero and indicated outer-sphere Li^+ complexes with a non-axial symmetry.

Because the inner-sphere complexes are localized above the siloxane ditrigonal cavities (Greathouse and Sposito, 1998) in the vicinity of the tetrahedral Al substitutions, the geometrical environment might also be influenced by the *trans*-vacant octahedral sheets. Separation of the influence of the tetrahedral charge location and *trans*-vacant octahedral sheet can only be obtained from studying pure *cis*- and *trans*-vacant montmorillonites with a high ξ value where hydrated Li^+ also form inner-sphere complexes.

After heating, the environment of Li^+ was no longer determined by the surrounding water molecules but by the atoms of the 2:1 layers. Although ηCS changed only slightly after dehydration, a decreasing δ^7Li indicated a more symmetric environment of Li^+ with increasing temperature up to 250ºC. After heating at 300ºC, the symmetry of the geometrical environment was again reduced slightly.

SUMMARY

Detailed characterization of five Li^+-saturated dioctahedral smectites of different chemical composition and ξ distribution, as well as the characterization of the samples obtained after heating at 110 to 300ºC, by a variety of techniques, provide new understanding of the influence of structural and morphological differences on the extent of CEC reduction of heated Li^+-saturated montmorillonites. This study showed that the well-known Hofmann-Klemen effect that is associated with reduced CEC and reduced hydration is related to the structural variety (*cis*- and *trans*-vacant) and the 2:1 layer dimension of the dioctahedral smectites.

The smectites studied could be classified as montmorillonite, beidellitic montmorillonite, and montmorillonitic beidellite. All samples are low-charged. The structure of the octahedral sheet varied from *cis*-vacant to *cis-trans*-vacant to *trans-cis*-vacant.

The CEC of the Li^+-exchanged samples after heating to 300ºC reflected the remaining CEC at the edges of the particles, and thus, the lateral size or aspect ratio of the 2:1 layers. The RCM obtained were stable over a period of at least 2 y.

The FWHM of the main ^7Li resonance indicated the migration of Li^+ into the pseudohexagonal cavities of the tetrahedral sheet and not into the octahedral vacancies for RCM. The shift of the δ of ^{29}Si and $^{27}Al^{IV}$ also supported the migration of Li^+ into the pseudohexagonal cavities of the tetrahedral sheet. The analysis of the CSA tensor of the ^7Li MAS NMR spectra revealed inner-sphere complexes of the hydrated interlayer Li^+ for smectites of the montmorillonite–beidellite series with 33% tetrahedral charge. After heating to 300ºC all RCM reached the state of thermodynamic stability (fully dehydrated interlayer Li^+) with ηCS = 1.

ACKNOWLEDGMENTS

Many thanks to Clariant Produkte (Deutschland) GmbH (formerly SÜD-CHEMIE AG), for supplying the bentonite samples. The authors acknowledge Nora Groschopf (University of Mainz) for the XRF analysis and are grateful to Marita Heinle for the ICP-OES measurements. Many thanks to Laure Delavernhe for discussions regarding the edge-charge distributions. The authors acknowledge Franz Rinderknecht for assistance with several chemical calculations and thank Fritz Wagner (Technical University of Munich) for performing the Mössbauer measurements. They are also grateful to Peter Weidler for Ar adsorption measurements and for discussions about surface and Mössbauer measurements. Finally, the authors thank Michael A. Velbel, Jana Madejová and the anonymous reviewers for valuable comments which improved the manuscript.

REFERENCES

Alba, M.D., Alvero, R., Becerro, A.I., Castro, M.A., and Trillo, J.M. (1998) Chemical behavior of lithium ions in reexpanded Li-montmorillonite. *The Journal of Physical Chemistry (B)*, **102**, 2207–2213.

Alvero, R., Alba, M.D., Castro, M.A., and Trillo, J.M. (1994) Reversible migration of lithium in montmorillonite. *The Journal of Physical Chemistry*, **98**, 7848–7853.

Bak, M., Ramussen, J.T., and Nielsen, N.C. (2000) SIMPSON: A general simulation program for solid-state NMR spectroscopy. *Journal of Magnetic Resonance*, **147**, 296–330.

Becerro, A.I., Mantovani, M., and Escudero, A. (2009) Mineralogical stability of phyllosilicates in hyperalkaline fluids: Influence of layer nature, octahedral occupation and presence of tetrahedral Al. *American Mineralogist*, **94**, 1187–1197.

Begaudeau, K., Morizet, Y., Florian, P., Paris, M., and Mercier, J.-C. (2012) Solid-state NMR analysis of Fe-bearing minerals: Implications and applications for earth sciences. *European Journal of Mineralogy*, **24**, 535–550.

Betega de Paiva, L., Morales, A.R., and Diaz, F.R.V. (2008) Organoclays: Properties, preparation and applications. *Applied Clay Science*, **42**, 8–24.

Breen, C., Madejová, J., and Komadel, P. (1995) Characterisation of moderately acid-treated, size-fractionated montmorillonites using IR and MAS NMR spectroscopy and thermal analysis. *Journal of Materials Chemistry*, **5**, 469–474.

Breen, C., Watson, R., Madejová, J., Komadel, P., and Klapyta, Z. (1997) Acid-activated organoclays: Preparation, characterization and catalytic activity of acid-treated tetra-alkyammonium exchanged smectites. *Langmuir*, **13**, 6473–6479.

Brunauer, S., Emmett, P.H., and Teller, E. (1932) Adsorption of gases in multimolecular layers. *Journal of the American Chemical Society*, **60**, 309–319.

Bujdák, J., Slosiariková, H., Nováková, L., and Čičel, B. (1991) Fixation of lithium cations in montmorillonite. *Chemical Papers*, **45**, 499–507.

Cadars, S., Guégan, R., Garaga, M.N., Bourrat, X., Le Forestier, L., Fayon, F., Huynh, T.V., Allier, T., Nour, Z., and Massiot, D. (2012) New insights into the molecular structures, compositions, and cation distributions in synthetic and natural montmorillonite clays. *Chemistry of Materials*, **24**, 4376–4389.

Calvet, R. and Prost, R. (1971) Cation migration into empty octahedral sites and surface properties of clays. *Clays and Clay Minerals*, **19**, 175–186.

Carroll, D. and Starkey, H.C. (1971) Reactivity of clay minerals with acids and alkalis. *Clays and Clay Minerals*, **19**, 321–333.

Chang, F.-R.C., Skipper, N.T., and Sposito, G. (1997) Monte Carlo and molecular dynamics simulations of interfacial structure in lithium-montmorillonite hydrates. *Langmuir*, **13**, 2074–2082.

Delavernhe, L., Steudel, A., Darbha, G.K., Schäfer, T., Schuhmann, R., Wöll, C., Geckeis, H., and Emmerich, K. (2015) Influence of mineralogical and morphological properties on the cation exchange behavior of dioctahedral smectites. *Colloids and Surfaces A: Physicochemical and Engineering Aspects*, **481**, 591–599.

Drits, V.A., Besson, G., and Muller, F. (1995) An improved model for structural transformations of heat-treated aluminous dioctahedral 2:1 layer silicates. *Clays and Clay Minerals*, **43**, 718–731.

Eisenhour, D.D. and Brown, R.K. (2009) Bentonite and its impact on modern life. *Elements*, **5**, 83–88.

Emmerich, K., Madson, F.T., and Kahr, G. (1999) Dehydroxylation behavior of heat-treated and steam-treated homoionic *cis*-vacant montmorillonites. *Clays and Clay Minerals*, **47**, 591–604.

Emmerich, K. (2011) Thermal analysis in the characterization and processing of industrial minerals. Pp. 129–170 in: *Advances in the Characterization of Industrial Minerals* (G.E. Christidis, editor). Volume **9**, EMU Notes in Mineralogy, European Mineralogical Union and the Mineralogical Society of Great Britain & Ireland, Twickenham, UK.

Emmerich, K., Plötze, M., and Kahr, G. (2001) Reversible collapse and Mg^{2+} release of de- and rehydroxylated homoionic *cis*-vacant montmorillonites. *Applied Clay Science*, **19**, 143–154.

Emmerich, K., Wolters, F., Kahr, G., and Lagaly, G. (2009) Clay profiling: The classification of montmorillonites. *Clays and Clay Minerals*, **57**, 104–114.

Fysh, S.A., Cashion, J.D., and Clark, P.E. (1983) Mössbauer effect studies of iron in kaolin: I Structural iron. *Clays and Clay Minerals*, **31**, 285–292.

Gates, W.P., Komadel, P., Madejová, J., Bujdák, J., Stucki, J.W., and Kirkpatrick, R.J. (2000) Electronic and structural properties of reduced-charge montmorillonites. *Applied Clay Science*, **16**, 257–271.

Greathouse, J. and Sposito, G. (1998) Monte Carlo and molecular dynamics studies of interlayer structure in $Li(H_2O)_3$ – smectites. *Journal of Physical Chemistry B*, **102**, 2406–2414.

Greene-Kelly, R. (1952) A test for montmorillonite. *Nature*, **170**, 1130–1131.

Gregg, S.J. and Sing, K.S.W. (1991) *Adsorption, Surface Area and Porosity*. Academic Press, London.

Harvey, C.C. and Lagaly, G. (2013) Industrial applications. Pp. 451–490 in: *Handbook of Clay Science – Part B Techniques and Applications* (F. Bergaya and G. Lagaly, editors) second edition. Developments in Clay Science Volume **5B**, Elsevier, Oxford.

Hofmann, U. and Klemen, R. (1950) Verlust der Austauschfähigkeit von Lithium-Ionen an Bentonit durch Erhitzung. *Zeitschrift für Anorganische und Allgemeine Chemie*, **262**, 95–99.

Hrobáriková, J. and Komadel, P. (2002) Sorption properties of reduced charge montmorillonites. *Geologica Carpathica*, **53**, 93–98.

Hrobáriková, J., Madejová, J., and Komadel, P. (2001) Effect of heating temperature on Li-fixation, layer charge and properties of fine fractions of bentonites. *Journal of Materials Chemistry*, **11**, 1452–1457.

Jaynes, W.F. and Bigham, J.M. (1987) Charge reduction, octahedral charge, and lithium retention in heated, Li-saturated smectites. *Clays and Clay Minerals*, **35**, 440–448.

Jozefaciuk, G. and Bowanko, G. (2002) Effect of acid and alkali treatments on surface areas and adsorption energies of selected minerals. *Clays and Clay Minerals*, **50**, 771–783.

Karakassides, M.A., Madejová, J., Arvaiová, B., Bourlinos, A., Petridis, D., and Komadel, P. (1999) Location of Li(I), Cu(II) and Cd(II) in heated montmorillonite: evidence from specular reflectance infrared and electron spin resonance spectroscopies. *Journal of Materials Chemistry*, **9**, 1553–1558.

Kleeberg, R. and Bergmann, J. (2002) Quantitative phase analysis using the Rietveld method and a fundamental parameter approach. *Powder Diffraction*: *Proceedings of the II International School on Powder Diffraction*. IACS, Kolkata, India.

Komadel, P. (2003) Chemically modified smectites. *Clay Minerals*, **38**, 127–138.

Komadel, P., Janek, M., Madejová, J., Weekes, A., and Breen, C. (1997) Acidity and catalytic activity of mildly acid-treated Mg-rich montmorillonite and hectorite. *Journal of the Chemical Society, Faraday Transactions*, **93**, 4207–4210.

Komadel, P., Madejová, J., and Bujdák, J. (2005) Preparation and properties of reduced-charge smectites – A review. *Clays and Clay Minerals*, **53**, 313–334.

https://doi.org/10.1346/CCMN.2015.0630501 Published online by Cambridge University Press

Komarneni, S., Fyfe, C.A., Kennedy, G.J., and Strobl, H. (1986) Characterization of synthetic and naturally occurring clays by ^{27}Al and ^{29}Si magic-angle spinning NMR spectroscopy. *Journal of the American Ceramic Society*, **69**, C-45–47.

Köster, H.M. (1977) Die Berechnung kristallchemischer Strukturformeln von 2:1-Schichtsilikaten unter Berücksichtigung der gemessenen Zwischenschichtladungen und Kationenumtausch-kapazitäten, sowie der Darstellung der Ladungsverteilung in der Struktur mittels Dreiecks-koordinaten. *Clay Minerals*, **12**, 45–54.

Lagaly, G. (1994) Layer charge determination by alkylammonium ions. Pp. 1–46 in: *Layer Charge Characteristics of 2:1 Silicate Clay Minerals* (A.R. Mermut, editor). The Clay Minerals Society, Boulder, Colorado, USA.

Lagaly, G. and Weiss, A. (1971) Anordnung und Orientierung kationischer Tenside auf ebenen Silicatoberflächen Teil IV. *Kolloid-Zeitschrift und Zeitschrift für Polymere*, **243**, 48–55.

Lippmaa, E., Mägi, M., Samoson, A., Engelhardt, G., and Grimmer, A.-R. (1980) Structural studies of silicates by solid-state high-resolution ^{29}Si NMR. *Journal of the American Chemical Society*, **102**, 4889–4893.

Luca, V., Cardile, C.M., and Meinhold, R.H. (1989) High-resolution multinuclear NMR study of cation migration in montmorillonite. *Clay Minerals*, **24**, 115–119.

Madejová, J., Bujdák, J., Gates, W.P., and Komadel, P. (1996) Preparation and infrared spectroscopic characterization of reduced charge montmorillonite with various Li contents. *Clay Minerals*, **31**, 233–241.

Madejová, J., Arvaiová, B., and Komadel, P. (1999) FTIR spectroscopic characterization of thermally treated Cu^{2+}, Cd^{2+}, and Li^+ montmorillonites. *Spectrochimica Acta Part A*, **55**, 2467–2476.

Madejová, J., Bujdák, J., Petit, S., and Komadel, P. (2000) Effects of chemical composition and temperature of heating on the infrared spectra of Li-saturated dioctahedral smectites. (I) Mid-infrared region. *Clay Minerals*, **35**, 739–751.

Mägi, M., Lippmaa, E., Samoson, A., Engelhardt, G., and Grimmer, A.-R. (1984) Solid-state high-resolution silicon-29 chemical shifts in silicates. *Journal of Physical Chemistry*, **88**, 1518–1522.

Massiot, D., Fayon, F., Capron, M., King, I., Le Calvé, S., Alonso, B., Durand, J.-O., Bujoli, B., Gan, Z., and Hoatson, G. (2002) Modelling one- and two-dimensional solid state NMR spectra. *Magnetic Resonance in Chemistry*, **40**, 70–76.

Mehra, O.P. and Jackson, M.L. (1960) Iron oxide removal from soils and clays by dithionite-citrate-system buffered with sodium bicarbonate. *7th National Conference on Clays and Clay Minerals*, 317–327.

Meier, L.P. and Kahr, G. (1999) Determination of the cation exchange capacity (CEC) of clay minerals using the complexes of copper(II) ion with triethylenetetramine and tetraethylenepentamine. *Clays and Clay Minerals*, **47**, 386–388.

Mignon, P., Ugliengo, P., Sodupe, M., and Hernandez, E.R. (2010) Ab initio molecular dynamics study of the hydration of Li^+, Na^+, and K^+ in a montmorillonite model. Influence of isomorphic substitution. *Physical Chemistry Chemical Physics*, **12**, 688–697.

Mosser, C., Michot, L.J., Villieras, F., and Romeo, M. (1997) Migration of cations in copper(II)-exchanged montmorillonite and laponite upon heating. *Clays and Clay Minerals*, **45**, 789–802.

Murad, E. (1998) Clays and clay minerals: What can Mössbauer spectroscopy do to help understand them? *Hyperfine Interactions*, **117**, 39–70.

Murad, E. and Johnston, J.H. (1987) Iron oxides and oxyhydroxides. Pp. 507–582 in: *Mössbauer Spectroscopy Applied to Inorganic Chemistry* (G.J. Long, editor). Vol. 2, Plenum, New York.

Murad, E. and Schwertmann, U. (1986) Influence of Al substitution and crystal size on the room-temperature Mössbauer spectrum of hematite. *Clays and Clay Minerals*, **34**, 1–6.

Novák, I. and Číčel, B. (1978) Dissolution of smectites in hydrochloric acid: II. Dissolution rate as a function of crystallochemical composition. *Clays and Clay Minerals*, **26**, 341–344.

Oldfield, E., Kinsey, R.A., Smith, K.A., Nichols, J.A., and Kirkpatrick, R.J. (1983) High-resolution NMR of inorganic solids – influence of magnetic centers on magic-angle sample-spinning lineshapes in some natural aluminosilicates. *Journal of Magnetic Resonance*, **51**, 325–329.

Olis, A.C., Malla, P.B., and Douglas, L.A. (1990) The rapid estimation of the layer charges of 2:1 expanding clays from a single alkylammonium ion expansion. *Clay Minerals*, **25**, 39–50.

Petrick, K. (2011) How does mineralogy control the technical properties of paper kaolins and ceramic clays? PhD thesis, Fakultät für Bauingenieur-, Geo- und Umweltwissenschaften, Universität Karlsruhe, Germany.

Sanz, J. and Robert, J.-L. (1992) Influence of structural factors on ^{29}Si and ^{27}Al NMR chemical shifts of phyllosilicates 2:1. *Physics and Chemistry of Minerals*, **19**, 39–45.

Sanz, J. and Serratosa, J.M. (1984) ^{29}Si and ^{27}Al high-resolution MAS-NMR spectra of phyllosilicates. *Journal of the American Chemical Society*, **106**, 4790–4793.

Schultz, L.G. (1969) Lithium and potassium absorption, dehydroxylation temperature, and structural water content of aluminous smectites. *Clays and Clay Minerals*, **17**, 115–149.

Skipper, N.T., Sposito, G., and Chang, F.-R.C. (1995) Monte Carlo simulation of interlayer molecular structure in swelling clay minerals. 2. Monolayer hydrates. *Clays and Clay Minerals*, **43**, 294–303.

Skoubris, E.N., Chryssikos, G.D., Christidis, G.E., and Gionis, V. (2013) Structural characterization of reduced-charge montmorillonites – evidence based on FTIR spectroscopy, thermal behavior, and layer-charge systematics. *Clays and Clay Minerals*, **61**, 83–97.

Sposito, G., Prost, R., and Gaultier, J.P. (1983) Infrared spectroscopic study of adsorbed water on reduced-charge montmorillonites. *Clays and Clay Minerals*, **31**, 9–16.

Steudel, A. (2009) Selection strategy and modification of layer silicates for technical applications. PhD thesis, Karlsruher Mineralogische und Geochemische Hefte (36), Schriftenreihe des Instituts für Mineralogie und Geochemie, Universität Karlsruhe (TH), Germany.

Steudel, A., Batenburg, L.F., Fischer, H.R., Weidler, P.G., and Emmerich, K. (2009) Alteration of swelling clay minerals by acid activation. *Applied Clay Science*, **44**, 105–115.

Steudel, A. and Emmerich, K. (2013) Strategies for the successful preparation of homoionic smectites. *Applied Clay Science*, **75-76**, 13–21.

Theng, B.K.G., Hayashi, S., Soma, M., and Seyama, H. (1997) Nuclear magnetic resonance and X-ray photoelectron spectroscopic investigation of lithium migration in montmorillonite. *Clay and Clay Minerals*, **45**, 718–723.

Tkáč, I., Komadel, P., and Müller, D. (1994) Acid-treated montmorillonites – A study by ^{29}Si and ^{27}Al MAS NMR. *Clay Minerals*, **29**, 11–19.

Tournassat, C., Neaman, A., Villiéras, F., Bosbach, D., and Charlet, L. (2003) Nanomorphology of montmorillonite particles: Estimation of the clay edge sorption site density by low-pressure gas adsorption and AFM observations.

American Mineralogist, **88**, 1989–1995.

Tributh, H. and Lagaly, G. (1986a) Aufbereitung und Identifizierung von Boden und Lagerstättentonen Teil I – Aufbereitung der Proben im Labor. *GIT Fachzeitschrift für das Laboratorium*, **30**, 524–529.

Tributh, H. and Lagaly, G. (1986b) Aufbereitung und Identifizierung von Boden und Lagerstättentonen Teil II – Korngrößenanalyse und Gewinnung von Tonsubfraktionen. *GIT Fachzeitschrift für das Laboratorium*, **30**, 771–776.

Trillo, J.M., Alba, M.D., Alvero, R., and Castro, M.A. (1993) Reexpansion of collapsed Li-montmorillonite; Evidence on the location of Li^+ ions. *Journal of the Chemical Society, Chemical Communications*, **24**, 1809–1811.

Wagner, F.E. and Kyek, A. (2004) Mössbauer spectroscopy in archeology: Introduction and experimental considerations. *Hyperfine Interactions*, **154**, 5–33.

Wang, J., Zeng, F.G., and Wang, J.X. (2006) Molecular dynamics simulation studies of interlayered structure in lithium-, sodium- and potassium-montmorillonite hydrate. *Acta Chimica Sinica*, **64**, 1654–1658.

Weiss, C.A. (Jr.), Altaner, S.P., and Kirkpatrick, R.J. (1987) High-resolution ^{29}Si NMR spectroscopy of 2:1 layer silicates: Correlations among chemical shift, structural distortions, and chemical variations. *American Mineralogist*, **72**, 935–942.

White, G.N. and Zelazny, L.W. (1988) Analysis and implications of the edge structure of dioctahedral phyllosilicates. *Clays and Clay Minerals*, **36**, 141–146.

Whitney, D.L. and Evans, B.W. (2010) Abbreviations for names of rock-forming minerals. *American Mineralogist*, **95**, 185–187.

Wolters, F. (2005) Classification of montmorillonites. PhD. thesis, Fakultät für Bauingenieur-, Geo- und Umweltwissenschaften, Universität Karlsruhe, Germany.

Wolters, F. and Emmerich, K. (2007) Thermal reactions of smectites – relation of dehydroxylation temperature to octahedral structure. *Thermochimica Acta*, **462**, 80–88.

Wolters, F., Lagaly, G., Kahr, G., Nüesch, R., and Emmerich, K. (2009) A comprehensive characterization of dioctahedral smectites. *Clays and Clay Minerals*, **57**, 115–133.

Xi, Y., Ding, Z., He, H., and Frost, R.L. (2004) Structure of organoclays – an X-ray diffraction and thermogravimetric analysis study. *Journal of Colloid and Interface Science*, **277**, 116–120.

(*Received 2 February 2015; revised 9 October 2015; Ms. 954; AE: J. Madejová*)